

Kinetic Advantage of Intrinsically Disordered Proteins in Coupled Folding–Binding Process: A Critical Assessment of the “Fly-Casting” Mechanism

Yongqi Huang and Zhirong Liu*

College of Chemistry and Molecular Engineering, Center for Theoretical Biology, State Key Laboratory for Structural Chemistry of Unstable and Stable Species, Peking University, Beijing 100871, China

Beijing National Laboratory for Molecular Sciences, Peking University, Beijing 100871, China

Received 16 April 2009;
received in revised form
29 June 2009;
accepted 4 September 2009
Available online
10 September 2009

Intrinsically disordered proteins (IDPs) are recognized to play important roles in many biological functions such as transcription and translation regulation, cellular signal transduction, protein phosphorylation, and molecular assemblies. The coupling of folding with binding through a “fly-casting” mechanism has been proposed to account for the fast binding kinetics of IDPs. In this article, experimental data from the literature were collated to verify the kinetic advantages of IDPs, while molecular simulations were performed to clarify the origin of the kinetic advantages. The phosphorylated KID–kinase-inducible domain interacting domain (KIX) complex was used as an example in the simulations. By modifying a coarse-grained model with a native-centric G α -like potential, we were able to continuously tune the degree of disorder of the phosphorylated KID domain and thus investigate the intrinsic role of chain flexibility in binding kinetics. The simulations show that the “fly-casting” effect is not only due to the greater capture radii of IDPs. The coupling of folding with binding of IDPs leads to a significant reduction in binding free-energy barrier. Such a reduction accelerates the binding process. Although the greater capture radius has been regarded as the main factor in promoting the binding rate of IDPs, we found that this parameter will also lead to the slower translational diffusion of IDPs when compared with ordered proteins. As a result, the capture rate of IDPs was found to be slower than that of ordered proteins. The main origin of the faster binding for IDPs are the fewer encounter times required before the formation of the final binding complex. The roles of the interchain native contacts fraction (Q_b) and the mass–center distance (ΔR) as reaction coordinates are also discussed.

© 2009 Elsevier Ltd. All rights reserved.

Keywords: “fly-casting” mechanism; intrinsically disordered protein; coupled folding–binding; coarse-grained simulation; capture radius

Edited by M. Levitt

Introduction

The unique three-dimensional structure of a protein has long been held as a prerequisite of

biological function. However, this structure–function paradigm has been challenged by the discovery of intrinsically disordered proteins (IDPs).¹ IDPs are expected to commonly exist in various proteomes. Bioinformatics studies have predicted that up to 5% of prokaryotic genomes and 30% of eukaryotic genomes encode proteins with wholly or partially unstructured domains.^{2,3} The percentage of IDPs is much higher when focusing on disease-related proteins,⁴ protein–protein interaction networks,⁵ and gene transcriptions.⁶ Although IDPs are disordered under physiological conditions, they are functionally important.⁷ They are involved in various critical physiological processes such as transcription and translation regulation,⁸ cellular signal transduction, protein phosphorylation, and

*Corresponding author. E-mail address:
LiuZhiRong@pku.edu.cn.

Abbreviations used: IDP, intrinsically disordered protein; KID, kinase-inducible domain; pKID, phosphorylated KID; KIX, kinase-inducible domain interacting domain; MFPT, mean first passage time; MPT, mean passage time; SA, spectrophotometric assay; SPR, surface plasmon resonance; SF, stopped flow; RMB, resonant mirror biosensor; QCM, quartz crystal microbalance.

molecular assemblies.⁹ In many cases, IDPs undergo conformational transitions to folded forms upon binding to their biological targets.¹⁰ This transition is referred to as “coupled folding and binding.”⁹ Among the increasing examples of coupled folding and binding,^{11–17} the kinase-inducible domain (KID) of the transcription factor cAMP response-element binding protein is one of the best characterized.^{18–21} Following phosphorylation at Ser133 in KID, phosphorylated KID (pKID) binds directly to the kinase-inducible domain interacting domain (KIX) of the cAMP response-element binding protein.¹⁸ Free pKID is intrinsically disordered but folds into two α -helices upon binding to KIX.²⁰ An NMR study has suggested that pKID forms an ensemble of transient encounter complexes after binding to the KIX domain and subsequently evolves to the intermediate state and, finally, to the native bound complex.²¹

The lack of folded structure in solution has been proposed to provide IDPs with several advantages over ordered proteins such as (i) conformational flexibility to interact with several targets,¹¹ (ii) increased interaction surface,²² (iii) rapid protein turnover,¹ and (iv) high specificity with low-affinity binding.²³ In particular, it has been proposed by Shoemaker *et al.* that being unstructured facilitates the binding of the IDPs to targets through the so-called “fly-casting” mechanism.²⁴ In this model, IDPs have greater capture radii than ordered proteins due to greater chain flexibilities. Thus, a flexible region of the disordered protein will partially and weakly bind to its partner from a large distance and then will reel in the binding partner while completing the folding simultaneously, thereby enhancing association (binding) speed. “Fly casting” also presents a route for the kinetic specificity of IDPs.

Although there are growing experimental studies on the kinetics of the coupled folding–binding process,^{13,17,21,25–33} it remains poorly determined whether IDPs possess higher binding rates than ordered proteins and whether the speeding effect operates via the “fly-casting” mechanism. Some studies have indicated that IDPs bind faster than their rigid counterparts.^{25,27,29} In the MICA example (a histocompatibility-complex-like protein that undergoes a disorder-to-order transition upon binding to its immunoreceptor NKG2D), 10 mutants designed to destabilize the receptor-bound complex were all found to accelerate the binding on-rates.²⁷ For chorismate mutase from *Methanococcus jannaschii*, when it was engineered into a molten globule, the ligand binding rate was speeded up by roughly threefold.²⁵ In contrast, there are studies that have reached the opposite conclusions.^{28,31} In the case of the PDZ domain family, while a correlation between association rate constants and protein stability was observed, the rate of binding was shown to increase with increasing stability.³¹ For the coupled folding and binding of apomyoglobin with hemin dicyanide, formation of the complex was not accelerated by an increase in structural disorder,²⁸ indicating that whether or not a protein

benefits kinetically from the “fly-casting” effect depends on a number of factors such as the capability of a ligand to act as a nucleation site for the folding process and the binding affinity of a ligand for the disordered regions of target proteins.

Despite the elegant picture provided by the “fly-casting” mechanism, the role of structural disorder in the binding kinetics of IDPs is not fully understood from a theoretical perspective. Theoretical analyses and computer simulations have been widely applied to investigate the coupled folding and binding process;^{24,34–43} however, little effort has been exerted to critically test the central point of the “fly-casting” mechanism: Do IDPs bind faster than ordered proteins? The greater capture radius of IDPs is an obvious advantage in binding kinetics. However, some other factors are possibly overlooked in such a simplified model. One obvious disadvantage of IDPs that we want to point out here is the translational diffusion coefficient D . IDPs will diffuse more slowly than ordered proteins due to their greater capture radii. The influence of the slower diffusion on the kinetic behaviors of IDPs is unclear. This parameter has not been considered in most research efforts where kinetic behaviors were extracted from free-energy profiles. To include the effect of D , we usually require direct kinetic simulations. Recently, Turjanski *et al.* simulated the coupled folding and binding of pKID to KIX, and they found that the binding rate of the prestructured form was lower than that of the unstructured form by ~ 1.6 -fold.³⁵ This provides valuable evidence about the kinetic advantages of IDPs; however, a detailed analysis is missing. As such, the separate roles of the capture radii and the diffusion constants remain unknown.

Here, we conducted a critical assessment of the “fly-casting” mechanism. Initially, experimental data on the binding kinetics of IDPs and ordered proteins were collected. A comparison showed that, on average, IDPs bind faster to their targets than ordered proteins. This observation is consistent with the “fly-casting” mechanism. Coarse-grained molecular dynamics simulations were then performed using a continuum G α -like C α chain model of the pKID–KIX complex. This simulation aimed to gain microscopic insights into the relationship between the chain disorder and the kinetic behavior of the pKID–KIX complex. Calculations indicate that disordered proteins bind to and unbind from target proteins through lower free-energy barriers and, therefore, with greater on-rates and off-rates under the transition temperature. Although the greater capture radii of IDPs increase the binding rate, their contribution to binding kinetics is not dominant, and the speeding effect due to the greater capture radii is essentially negated by the slower diffusion in the encounter processes. The main origin of the kinetic advantage of IDPs is that the lower free-energy barriers enable encounter complexes to have a greater probability

of evolving to the final bound states (i.e., IDPs require a smaller number of encounters to accomplish the binding process).

Results

Experimental data suggest the accelerated binding effect of IDPs

Protein binding rates cover a wide range of magnitudes and are influenced by a number of factors (e.g., electrostatic interactions and nonspecific binding; in the latter case, a protein first binds nonspecifically to the full surface of the target and then searches for the final specific binding sites within a reduced phase space).⁴⁴ For a comparison of the different binding kinetics between IDPs and

ordered proteins, the two systems should be compared under similar conditions, or large data sets should be used to average out the influence of other factors. Kinetic data on protein–protein associations for 45 ordered proteins and 35 IDPs were collected from the literature (Tables 1 and 2). The analysis is presented in Fig. 1. To our best knowledge, such an approach has not been previously carried out in a systematic fashion. Although our database is incomplete, this analysis reveals a number of distinct kinetic features for IDPs and ordered proteins. In Fig. 1, the binding rates are plotted as a function of stability because a comparison is only meaningful under the same stability conditions meaning that an increase in binding stability usually enhances binding kinetics. In general, Fig. 1 shows that there is no clear separation between IDPs and ordered proteins. For both IDPs and ordered proteins, k_{on} and k_{off} cover

Table 1. Kinetic data for ordered complex

Ordered complex	k_{on} ($10^5 \text{M}^{-1} \text{s}^{-1}$)	k_{off} (s^{-1})	K_{d} (nM)	Method	Reference
IgG/anti-IgG	52.5	0.08	15	Fluorescence correlation spectroscopy	78
BPTI/trypsin	9.9	0.00000005	0.00005	SA	79
BPTI/chymotrypsin	1.7	0.0018	11	SA	79
E225/D1.3	0.01	0.00036	360	SPR	80
FVIIa/sTF	3.4	0.0021	6.3	SPR	81
hIL5/shIL5R α -Fc	4.9	0.0037	7.6	SPR	82
hGH/hGPbp	3	0.00027	0.9	SPR	83
sCD4/gp120	0.83	0.0016	19	SPR	84
CD4/gp120	0.672	0.0015	22	SPR	85
g5p/Trx-(SH)2	0.47	0.000105	2.2	SPR	86
Cytochrome <i>c</i> /2B5	6.5	0.00008	0.12	SF	87
Cytochrome <i>c</i> /5F8	15	0.0001	0.067	SF	87
SUA-rIgG/Ecto-Tva	2.76	0.0045	16.4	RMB	88
I α I/trypsin (human)	110	0.7	64	Not clear	89
I α I/chymotrypsin (bovine)	2.2	0.00053	2.4	Not clear	89
AMY2/BAS1	1.19	0.0002	1.7	SPR	90
Myosin/CaM	460	1.0	22	SF	91
HEL/VL: :VH-MaIE	0.784	0.000666	8.46	SPR	92
HEL/VH: :VL-MaIE	0.866	0.000751	8.96	SPR	92
Barstar/barnase	6000	0.000008	0.000013	SF	93
B-CheZ/CheY	56.4	0.04	7.1	SF	94
HyHEL/BWQL	180	0.96	53	SF	95
PI3-K/IGF-1R	4.83	0.00212	4.4	SPR	96
GroEL/GroES	8	0.011	14	SPR	97
smGN/CaM	12.4	0.0055	4.42	SPR	98
BoNT/scFv	20.9	0.0000942	0.0451	SPR	99
Palivizumab/Fab	1.26	0.000662	5.25	SPR	100
Palivizumab/IgG	1.27	0.00043	3.386	SPR	100
Fyn SH3/PRD1	0.77	0.41	5200	SPR	101
AChR/Fyn SH2	0.042	0.000008	1.9	RBA	102
AChR/Fyk SH2	0.062	0.000008	1.3	RBA	102
IgG/protein A/G	4.26	0.0000485	0.113	SPR	103
AR-AF1/RAF74	0.2	0.0033	170	SPR	104
p53/NPM	0.043	0.00135	314	SPR	105
Ras/Raf-RBD	355	1.7	50	SF	106
Stathmin/tubulin	0.089	0.005	560	SPR	107
IL5/sIL5R α	24	0.0072	3.1	SPR	108
IgG/CGRP α (human)	1.156	0.000671	5.78	SPR	109
hPRLr-ECD/hPRL	1.398	0.00062	4.4	SPR	110
hPRLr-ECD/hGH	0.3578	0.00023	6.7	SPR	110
IGF-II/IGF2R	6.62	0.0787	118.8	SPR	111
BLIP/TEM-1	2.4	0.00016	0.7	SPR	112
AF6 RA1/Ras	64	15.3	2400	SF	113
CD81LEL-GST/HCV	0.089	0.00047	52	SPR	114
CopY/ <i>cop</i> promoter	0.43	0.0000073	0.17	SPR	115

Table 2. Kinetic data for disordered complex

Disordered complex	k_{on} ($10^5\text{M}^{-1}\text{s}^{-1}$)	k_{off} (s^{-1})	K_{d} (μM)	Method	Reference
SH2/Y751	33.4	0.14	0.042	SPR	116
SH2/pYHmT	2	0.2	1	SPR	117
SH2/pY531	2	1	5	SPR	117
SH2/ITAM	41.7	0.0098	0.00234	Scintillation proximity-based assay	118
Grb2-mSos1/EGFR	63	0.197	0.031	SPR	119
Grb2-mSos1/IR-PEP	10.5	0.31	0.296	SPR	119
BRCA1-BRCT/bBACH1-P	40	0.02	0.005	SPR	120
Cdc42/WASP	1.9	0.0119	0.063	SPR	121
SUA/Ecto-Tva	0.56	0.0084	0.149	RMB	88
CaM/CKII	1300	0.26	0.002	SF	122
TolA/ColN	0.5	0.042	0.83	SPR	14
TolA/ColN	1.1	0.011	0.1	SF	123
TCR/pMHC	0.372	0.219	5.9	SPR	124
S-peptide/S-protein	180	0.000119	0.000006	SF	12
Sky/ β_3	0.48	0.00114	0.024	SPR	125
Sky/ β_2	0.38	20.00143	0.038	SPR	125
Sky/ β_1	0.19	0.00132	0.071	SPR	125
HIF/TAZ1	12,900	185	0.143	NMR	17
GCN4 D7A	80	0.0015	0.00019	SF	126
Ubf45W	0.031	0.00068	0.22	SF	126
GCN4	3000	0.072	0.00024	SF	127
GCN4-p1	27.5	0.153	0.056	SF	128
GCN4	6.63	0.17	0.26	SF	129
Leucine zipper	40	10	2.5	SF	130
KIX/pKID	0.0013	0.0014	10.8	QCM	131
KIX/KID	0.0012	0.025	208	QCM	131
MICA/NKG2D	0.075	0.013	1.7	SPR	27
AR-AF1/SRC-1	0.0024	0.0033	14	SPR	104
AR-AF1/RAP74-NTD	0.046	0.0012	0.63	SPR	104
E6/GST-E6AP	0.713	0.18	2.59	SPR	132
E6/MBP-E6AP	0.542	0.28	5.26	SPR	132
MEM-265/peptide	2.74	0.000575	0.0021	SPR	133
MDM2/p53	92	2.06	0.22	SF	134
Imp α /NLS	0.2	0.00031	0.0155	SPR	135
D-KQTSV/PSD-95PDZ3	79	6.2	0.8	SF	136

a range of 8–10 orders of magnitude. Moreover, the kinetic data collected have been measured under various conditions and techniques. Consequently, comparison of a single datum is insignificant. However, when the two data sets were fitted linearly under the constraint that their slopes are equal, the purpose of which is to reveal the difference in general trends between IDPs and ordered proteins, IDPs showed greater on-rates and off-rates than the ordered proteins. Estimated from the fitted lines, the k_{on} and k_{off} values of IDPs are ~ 2.9 times as large as those of ordered proteins. The slope of $\log_{10}(k_{\text{on}}) \sim \log_{10}(K_{\text{d}})$ is -0.36 , and the slope of $\log_{10}(k_{\text{off}}) \sim \log_{10}(K_{\text{d}})$ is 0.64 , implying that the on-rates are less sensitive to the stability of the complex than the off-rates. A Z-test was carried out to further quantitatively compare the kinetic difference between IDPs and ordered proteins. A moderate value of significance level (0.06) for the kinetic difference between IDPs and ordered proteins was obtained. Qualitatively, this comparison provides some insight into the kinetic advantages of IDPs, and a larger database with detailed analysis would aid any further studies. From a statistical analysis viewpoint, these data provide perhaps some supports that IDPs and ordered proteins exhibit distinct kinetic behaviors.

Simulations to continuously tune the protein structure from disordered to ordered

To explore how structural flexibility affects the binding kinetics of protein–protein interactions, we performed simulations on the formation of the pKID–KIX complex. An important aspect of the simulation work is that the potentials and conditions of the system are under complete control. This ensures that, by removing or altering specific elements, the roles of the potentials and conditions in determining a given property can be individually examined.⁴⁵ Here, the parameter α was introduced into a continuum explicit-chain model to tune the interactions within the disordered protein chain (pKID) without changing those between the disordered chain and the ordered chain (pKID and KIX) (see Models and Method). Systems with small α values have weaker driving forces to hold the pKID in a structured state, whereas large α values have stronger driving forces for facilitating the formation of structured conformations. Consequently, the α value can be changed to continuously tune pKID from the disordered state to the ordered state. In this way, one can separate the influence of structural flexibility on kinetics from other factors such as stability, topology, and binding specificity.

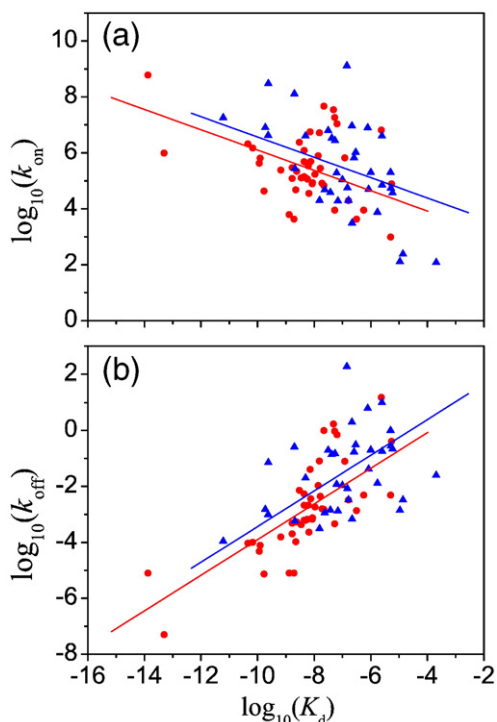


Fig. 1. The collection of binding kinetics data for IDPs (blue triangles) and ordered proteins (red circles). Forty-five and 35 data are collected for ordered and disordered proteins, respectively. Experimental details for the binding kinetics analyzed here can be found in the original references listed in Tables 1 and 2. Continuous lines are linear fits to the scattering data of IDPs and ordered proteins under the condition that the slopes are equal in (a) and (b), respectively. Since the dissociation constant K_d is equal to $k_{\text{off}}/k_{\text{on}}$, the difference between the slopes of (a) and (b) is exactly equal to 1.0.

Calculations on protein stability and flexibility validate the effect of α (Fig. 2). As discussed in Experimental Data Suggest the Accelerated Binding Effect of IDPs, a comparison of proteins with different flexibilities should be conducted under the same stability conditions. In Fig. 2a, heat capacity (C_p) curves of the pKID–KIX binding/unbinding process were plotted for various α values. At the transition temperature (T_m) defined as the temperature of the C_p peak, the pKID–KIX complex has an equal probability of being present in either the bound form or the unbound form, where the unbound form comprises unbound conformations ($Q_b=0$) with various mass-center distances between the two chains. The T_m value was found to shift to higher temperatures as α increases (Fig. 2a and b). A recent study also found that a rigid binding motif binds to the target at a higher transition temperature than a flexible binding motif.⁴⁶ The flexibility of pKID was examined by determining the average fraction of native intrachain contacts of pKID in the free form (i.e., in the absence of KIX) $\langle Q_f^{\text{free}} \rangle$ at the T_m (Fig. 2c). As expected, when α increases from 0.1 to 8.0, pKID is tuned from a disordered state ($\langle Q_f^{\text{free}} \rangle = 0.38$) to an

ordered state ($\langle Q_f^{\text{free}} \rangle = 0.91$). NMR data have shown that helix α_A of pKID is ~ 50 – 60% folded, and helix α_B is $\sim 15\%$ formed,⁴⁷ whereas some IDPs may have less than 10% of the folded contacts. For our current model, we could not decrease the fraction of residual native contacts to values as low as 10%. Increasing the intrachain interaction strength will enhance the thermal stability of the complex (Fig. 2d).

Ordered proteins dock to their targets through induced-fit or conformational selection,^{37,48} whereas IDPs bind to their targets coupled with folding²¹ (the binding of IDPs may also possess some components of conformational selection if they populate “preformed elements”,^{49,50} however, the preformed structures will be stabilized and folded further upon binding).⁵¹ Changing α values in our scheme regulates the system between coupled folding–binding and docking (Fig. 3). Consistent with the results from the energy landscape perspective,^{38,52} the folding and the binding of flexible proteins are intimately coupled (e.g., $\alpha=0.1$) (Fig. 3a). However, this coupling is weakened as chain flexibility decreases. Figure 3 shows clearly the evolution from coupled folding–binding to docking, indicating that no clear distinction between these two binding mechanisms exists. A simulation with the HP lattice model has also shown that both mechanisms can be observed in the binding process regardless of whether the protein is ordered or disordered, whereas the preference of binding mechanisms is different.³⁷ For weak intrachain interactions (e.g., $\alpha=0.1$), free pKID has only 38% of the native contacts and can be considered disordered. Initial weak binding with KIX domain ($Q_b \leq 0.2$) does not cause marked folding of the pKID domain. Significant folding takes place when the binding free-energy barrier is passed. For strong intrachain interactions (e.g., $\alpha=5.0$), free pKID has 85% of the native contacts and is essentially in the folded state. In this situation, docking was observed from the free proteins to the bound complex, and coupled folding was found to be very weak.

IDPs possess lower binding energy barriers and greater capture radii

To test the “fly-casting” effect for the coupled folding–binding process, we examined the binding free-energy profiles of the pKID–KIX complex at T_m . Regardless of whether Q_b or the mass-center distance between pKID and KIX (ΔR) was chosen as reaction coordinate, the binding free-energy barrier of systems with greater chain flexibility (lower α value) is always lower than that of systems with lower chain flexibility (Fig. 4). For the most disordered system ($\alpha=0.1$), the binding energy barrier is $2.4k_B T$ lower than that of the most ordered system ($\alpha=8.0$) if Q_b was used as the reaction coordinate, or $0.92k_B T$ if ΔR was used (Fig. 4a and b). In addition, the transition states of the

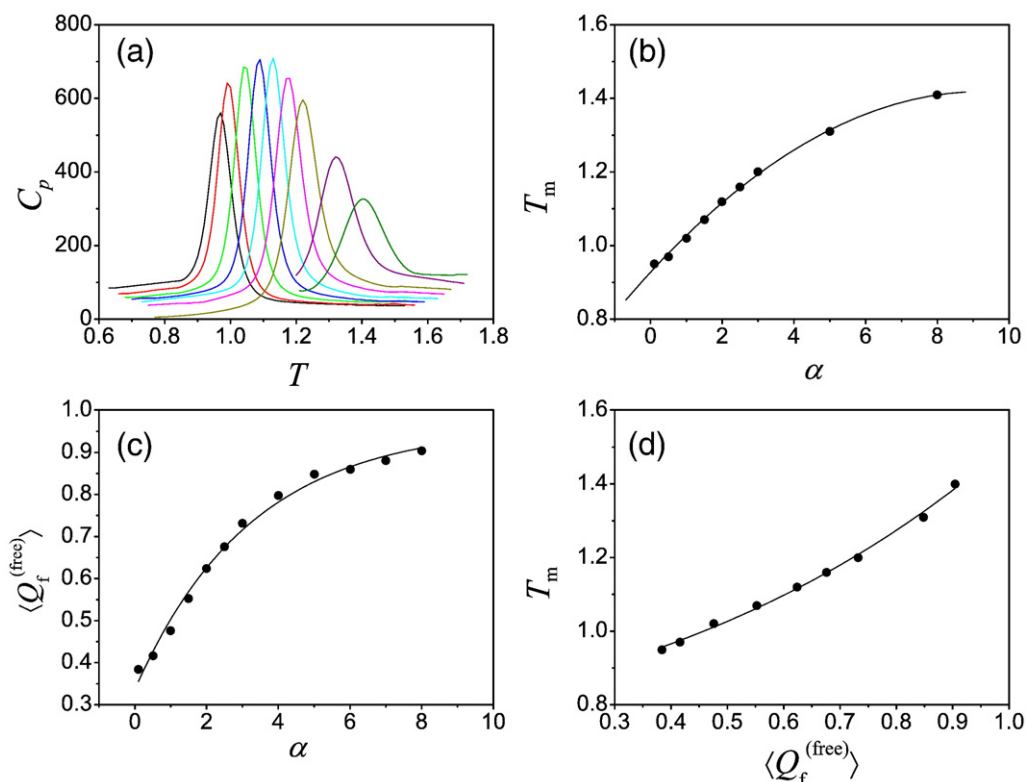


Fig. 2. Effect of parameter α on the stability and flexibility of the pKID–KIX complex and free pKID. (a) Heat capacity C_p of pKID–KIX binding/unbinding process as a function of temperature T for various α values (from left to right): 0.1, 0.5, 1.0, 1.5, 2.0, 2.5, 3.0, 5.0, and 8.0. C_p is computed from the density of states using histogram techniques with bias potential. Sampling is performed with a concentration of 200 μM for pKID–KIX, and this concentration is used throughout the article, except where specified. T is measured in units of ε_0/k_B , where k_B is the Boltzmann constant and ε_0 is an energy constant, as explained in [Models and Method](#). (b) The transition temperature T_m of the pKID–KIX binding/unbinding process as a function of α . T_m was determined as the temperature of the heat capacity peak in (a). (c) Average fraction of native intrachain contacts of pKID in the free form $\langle Q_f^{(free)} \rangle$ as a function of α under the transition temperature determined in (b). (d) Relationship between T_m and $\langle Q_f^{(free)} \rangle$.

disordered systems were found to have fewer interchain native contacts than those of the ordered systems (Fig. 4a). Interchain and intrachain native contacts have been found to be only partially formed in the intermediate state,²¹ and the difference within the transition states between the disordered proteins and the ordered proteins may account for their difference in binding mechanism and kinetics. Our results suggest that it is easier for disordered proteins to reach the transition state than ordered proteins. The free-energy profiles also reveal that when using ΔR as reaction coordinate, disordered proteins cross the free-energy barrier at a larger distance than ordered proteins (Fig. 4b). This indicates that disordered proteins have greater effective capture radii (Fig. 4d) (e.g., $\Delta R=29$ Å for $\alpha=0.1$ and $\Delta R=21$ Å for $\alpha=8.0$, with a ratio of 1.5). The results appear to support the “fly-casting” mechanism.

IDPs do not have greater capture rates than ordered proteins

In the “fly-casting” mechanism, the kinetic advantages of IDPs are usually interpreted as

their greater capture radii enabling faster encounter events to form weak binding complexes. This appealing interpretation, however, has not been tested rigorously. Here, capture events in pKID–KIX binding process were investigated. Due to a lack of a clear and unique definition of the encounter complex and capture event,⁵³ we used $Q_b > 0$ as criterion and started simulations from randomly chosen unbound states ($Q_b = 0$). An encounter complex state was defined when the system evolved from $Q_b = 0$ to $Q_b > 0$ (usually had only one interchain native contact). The average capture time (t_{cap}) to form the encounter complex is shown in Fig. 5a as a function of $\langle Q_f^{(free)} \rangle$. Remarkably, although IDPs have greater capture radii, Fig. 5a indicates that IDPs do not have greater capture rates than ordered proteins. On the contrary, it was found that the capture rate of the most disordered case is slower than that of the most ordered case by a ratio of ~ 1.4 (Fig. 5a, filled circles). In a comparison test, we used any two residues (one from pKID and the other from KIX) that were less than 8.0 Å apart as an encounter criterion and applied the 12–10 form nonbonded interactions (see Eq. (3)) to all

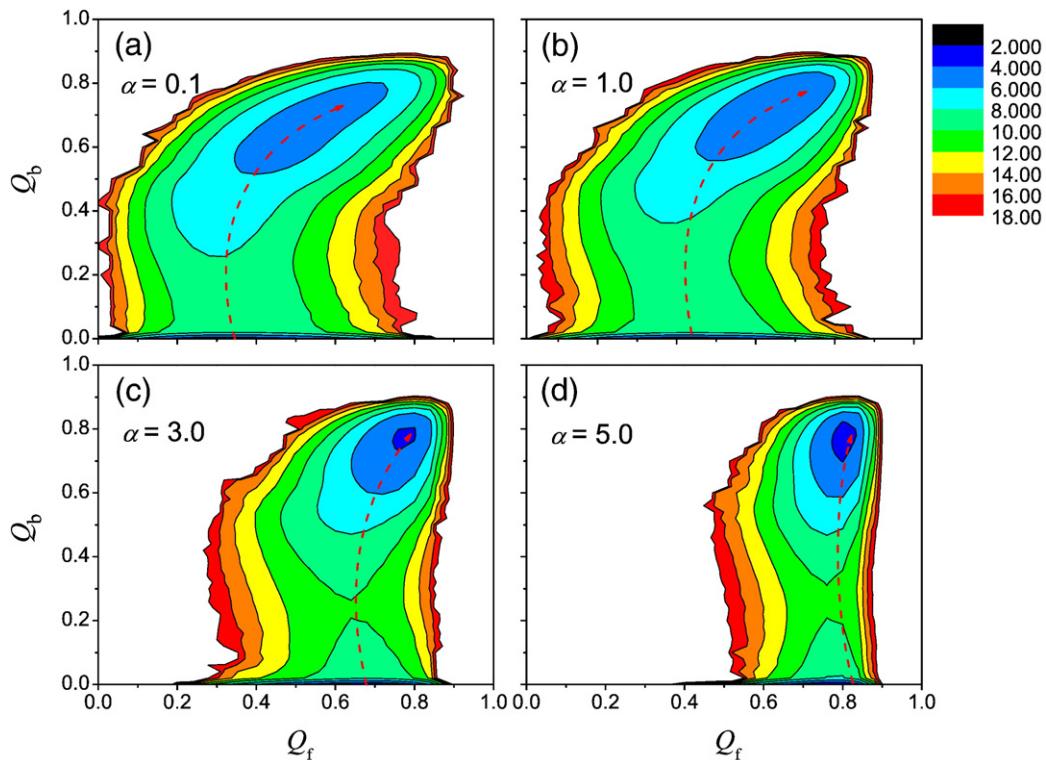


Fig. 3. Contour plots of the two-dimensional free-energy landscape (in units of $k_B T$) of the binding/unbinding process of the pKID–KIX complex as a function of the fraction of intrachain native contacts (Q_f) and the fraction of interchain native contacts (Q_b) at the transition temperature (T_m) for various α values: (a) $\alpha=0.1$, (b) $\alpha=1.0$, (c) $\alpha=3.0$, and (d) $\alpha=5.0$. Free energy is calculated as $F(Q_b, Q_f)/k_B T = -\ln[P(Q_b, Q_f)]$, where $P(Q_b, Q_f)$ is the normalized population distribution as a function of Q_b and Q_f . Evolution from coupled folding–binding to docking is clearly shown as the parameter α gradually increases (e.g., from 0.1 to 5.0). Binding paths are indicated by red broken lines from the unbound state to the bound state. The reaction coordinate Q_b treats all states with $Q_b=0$ as the same states because all unbound states possess zero interchain native contact ($Q_b=0$); however, they may have markedly different mass–center separations ΔR . Consequently, in these two-dimensional free-energy landscapes, states with $Q_b=0$ represent all unbound states with different ΔR values.

interchain residue pairs (i.e., regardless of native or nonnative pairs) (Fig. 5a, open diamonds). We also tested a scheme in which all interactions between pKID and KIX were switched off so that kinetics was merely controlled by diffusion and random collision, and we used the encounter criterion above (Fig. 5a, open triangles). The comparison tests showed trends similar to those of the original scheme (Fig. 5a). Therefore, the absence of a kinetic advantage for IDPs in the capture process is not an artifact of the Gō-like potential we have adopted or the criterion of the encounter complex.

We noted that slow diffusion will hamper IDPs from achieving a greater capture rate by a greater capture radius. Encounter events in our simulations were stochastic diffusion processes because long-range interactions were not included in our model. Diffusion simulations with pKID in free form showed that the diffusion coefficient D decreases when the degree of chain disorder increases (Fig. 5b). This property can be understood by considering that IDPs possess greater hydrodynamic radii.⁵⁴ After subtraction of the influence of D , systems with different chain flexibilities will have nearly the same capture rate

(data not shown), indicating that capture radius contributes little to increasing the capture rate. Therefore, greater capture radii and smaller diffusion rates for IDPs negate each other and, consequently, IDPs do not necessarily possess greater capture rates than ordered proteins. Including long-range interactions (e.g., favorable electrostatic interactions) in the binding process should increase the diffusion rate and may have a positive effect on the overall binding rate. The study of the binding kinetics influenced by electrostatic interactions would be interesting because IDPs contain more charged residues than globular proteins.⁵⁴ The electrostatic interactions were not included in the current model, and we did not pursue them in this article.

IDPs do have enhanced binding rates

Capture rates are closely related to binding rates, but they are not identical. Usually the binding rate is the measured quantity in experiments, and it is also the main criterion used to judge whether IDPs have any kinetic advantage over ordered proteins. To better understand the kinetic process, we

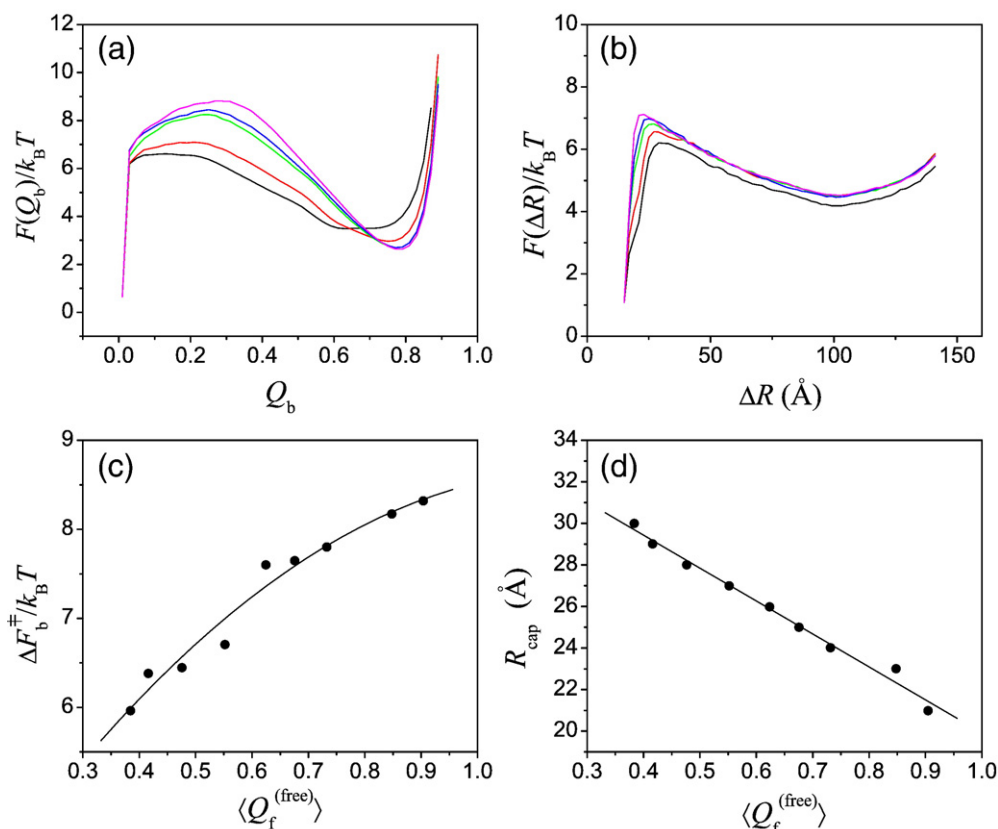


Fig. 4. (a and b) Free-energy profiles of pKID–KIX binding at T_m using the interchain native contacts fraction Q_b and the distance between the mass centers of the two chains ΔR as reaction coordinates for $\alpha=0.1, 1.0, 2.0, 3.0,$ and 5.0 (from bottom to top). Free energy is calculated as $F(x)/k_B T = -\ln[P(x)]$, where x indicates Q_b or ΔR , and $P(x)$ is the normalized population distribution obtained in simulations as a function of x . For convenience of comparison, free-energy profiles are slightly shifted to make states, with $Q_b=0$ (a) or $\Delta R=15$ Å (b) having the same value for various α . (c) The binding free-energy barrier ΔF_b^\ddagger (in units of $k_B T$) as a function of chain flexibility. ΔF_b^\ddagger is calculated as the difference between the peak value of $F(Q_b)$ and the value at $Q_b=0$ from (a). (d) Effective capture radius R_{cap} as a function of chain flexibility. R_{cap} is defined as the mass-center distance ΔR corresponding to the peak of the free-energy profile in (b).

calculated the binding and unbinding rates of the pKID–KIX complex near the transition temperatures (Fig. 6). Binding simulations were performed with 400 randomly chosen unbound states, with $Q_b=0$ obtained from high-temperature simulations. Binding was considered to occur when the system evolved to a state that met the minimum of the free energy around $Q_b \sim 0.8$ (as indicated in Fig. 3). Unbinding simulations were carried out with the native state, and unbinding was considered to occur when the system evolved to a state with $Q_b=0$ and with the mass-center separation between the two molecules $\Delta R > 45$ Å. As observed in the binding experiments, the simulated binding rates are concentration dependent (Fig. 6a), where the binding mean first passage time (MFPT) is linked to k_{on} by $\text{MFPT}^{-1} = k_{on} [\text{pKID}]$. The stability dependence of the binding/unbinding rates is exemplified in Fig. 6b. The binding and unbinding MFPTs were clearly found to exhibit chevron-like behaviors, which are similar to the simulation results performed on protein folding.⁵⁵ Transition temperatures extrapolated from binding/unbind-

ing kinetics are consistent with those defined by the C_p curves in Fig. 2a. The most informative result comes from the binding rate under the transition temperature when the protein is tuned from the disordered state to the ordered state (Fig. 6c). In contrast to the capture rate results, IDPs do exhibit a greater binding rate than ordered proteins (i.e., the binding rate for the disordered systems with $\alpha=0.1$ is ~ 2.5 times as fast as that for the ordered systems with $\alpha=8.0$). The enhanced binding kinetics revealed here qualitatively validates the conclusion based on free-energy calculation (Fig. 4), and it is consistent with the analysis on experimental data (Fig. 1) and expectation of the “fly-casting” mechanism.²⁴

Fewer encounter times: The origin of the kinetic advantages of IDPs

How can IDPs possess a greater binding rate yet have a slower capture rate compared with ordered proteins? To elucidate the origin of the kinetic

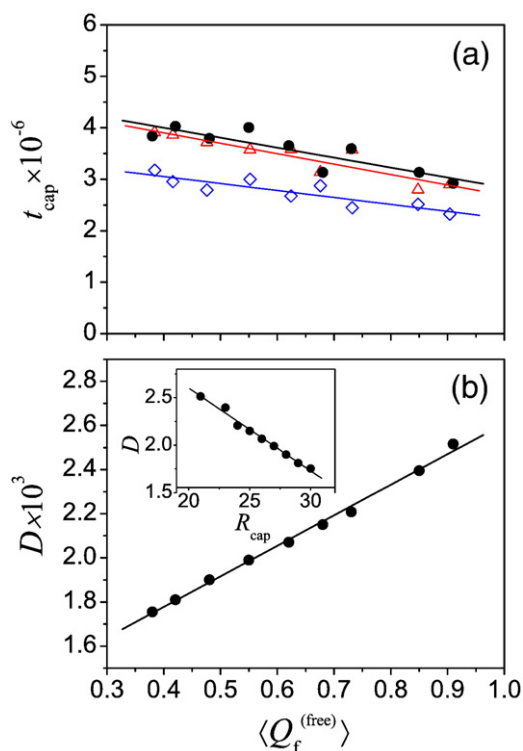


Fig. 5. Capture rates of pKID–KIX binding and the influence of translational diffusion. (a) Average capture time t_{cap} of pKID–KIX binding as a function of $\langle Q_f^{(\text{free})} \rangle$ at T_m (black circles). Each data point is determined from 400 capture trajectories starting from randomly unbound states. The corresponding data when interchain interactions are applied for all residue pairs (open diamonds) and when all interchain interactions are switched off (open triangles) are also shown. See the text for more details. (b) Diffusion constant D of the pKID mass center in free form as a function of $\langle Q_f^{(\text{free})} \rangle$ at T_m . D is calculated as $D = \langle x \rangle^2 / 2t$, and each data point is averaged from 10 long-time (5,000,000 steps) diffusion trajectories. Inset shows the diffusion coefficient D as a function of the capture radius R_{cap} .

advantages of IDPs, we decomposed the binding process into an encounter step and a further evolution step:



where pKID + KIX is the unbound state, pKID·KIX is the native bound state, and pKID⋯KIX is a loosely bound intermediate formed by the capture event (encounter complex). For each trajectory in our simulations, an unbound state ($Q_b = 0$) was the initial state, and the intermediate was reached when a native contact was formed ($Q_b > 0$). The intermediate state would then either escape to the unbound state when $Q_b = 0$ and $\Delta R > 45$ Å or evolve to the bound state when the system reached the minimum of the free energy ($Q_b \sim 0.8$; Fig. 3). A trajectory was terminated when the bound state was reached. Generally, to achieve the native bound state, the two

proteins have to encounter each other several times in a binding trajectory. By dissecting the binding trajectories into three states, we accumulated the transition number (N) and the average transition time [measured by the mean passage time (MPT)] between any two states. The escaping rate k_{esc} and the evolving rate k_{evo} were calculated as:

$$k_{\text{esc}} = [(\text{MPT}_{\text{esc}} \times N_{\text{esc}} + \text{MPT}_{\text{evo}} \times N_{\text{evo}}) \times N_{\text{esc}} / (N_{\text{esc}} + N_{\text{evo}})]^{-1} \quad (1)$$

$$k_{\text{evo}} = [(\text{MPT}_{\text{esc}} \times N_{\text{esc}} + \text{MPT}_{\text{evo}} \times N_{\text{evo}}) \times N_{\text{evo}} / (N_{\text{esc}} + N_{\text{evo}})]^{-1} \quad (2)$$

where MPT_{esc} is the mean passage time from the encounter state to the unbound state; MPT_{evo} is the mean passage time from the encounter state to the bound state; and N_{esc} and N_{evo} are the corresponding numbers of transitions.

Decomposition of the simulated trajectories is presented in Fig. 7. As chain flexibility increases, the escaping rate k_{esc} decreases and the evolving rate k_{evo} increases (Fig. 7a). As a result, encounter times (i.e., the mean number of times the two proteins have to encounter before forming the final complex), calculated as $k_{\text{esc}}/k_{\text{evo}} + 1$ or obtained from direct trajectory decomposition, was reduced (Fig. 7b). For disordered systems ($\alpha = 0.1$), only 3–4 encounter times are required; for ordered systems ($\alpha = 8.0$), 12 encounter times are required. Therefore, a faster capture rate does not ensure a greater binding rate for ordered proteins, since the encounter complex may escape to the unbound state but not evolve to the bound state. Our results unambiguously reveal that the increase in the binding rate of IDPs with target proteins is not due to the greater capture radii and capture rates, as originally proposed, but due to fewer encounter (capture) times required to accomplish the binding process. It should be noted that the definition of the encounter complex is not unique, and transition rates along with encounter times are sensitive to particular definitions. We tested various criteria of the encounter complex and confirmed that the general trend exhibited in Fig. 7 and the conclusions stated above do not change when the definition of the encounter complex is varied.

Discussion

IDPs have been found to be ubiquitous within many species, and the intrinsic chain flexibility associated with IDPs enables these proteins to bind to their targets with low affinity²³ and rapid kinetics.²⁴ Experimental detection of such interactions has been carried out under various binding conditions, making it difficult to directly compare the thermodynamics and kinetics between disordered

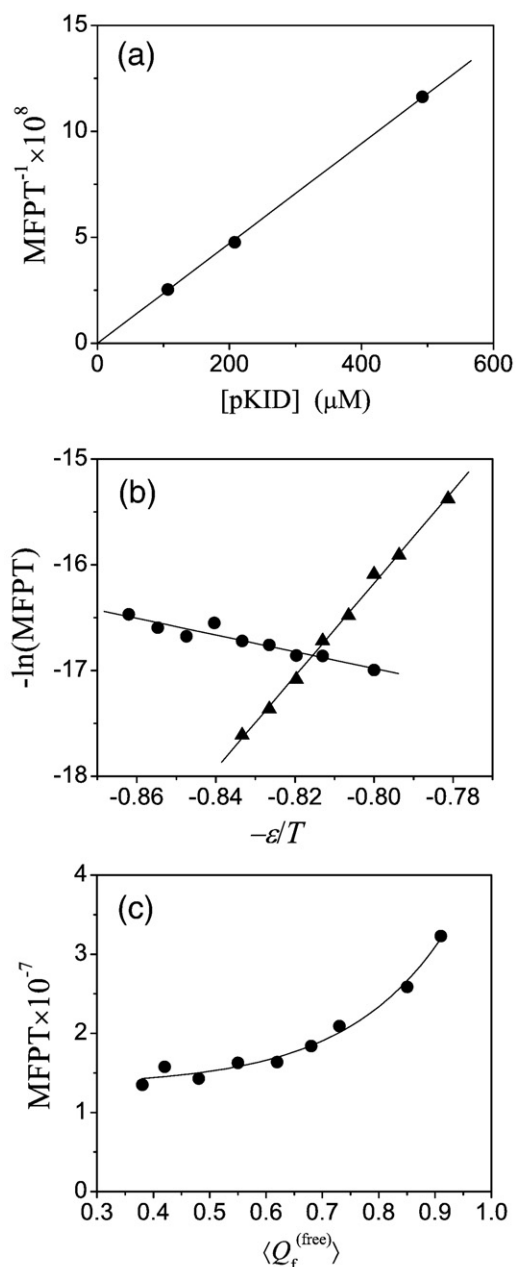


Fig. 6. Kinetics of the pKID–KIX binding/unbinding process. (a) Concentration dependence of the binding rate (as a reciprocal of MFPT) for $\alpha=3.0$ and $T=1.20$. (b) The chevron plot, minus the logarithm of the binding/unbinding MFPT as a function of $-\epsilon/T$, is shown for a system with $\alpha=3.0$. $[\text{pKID}] = 200 \mu\text{M}$ is used here. Binding and unbinding data points are represented by circles and triangles, respectively. (c) The average binding time as a function of chain flexibility at T_m .

and ordered proteins. Hence, simulations of protein binding with different chain flexibilities while keeping other conditions constant were performed in this article. This allowed a comparison of thermodynamic and kinetic properties under the same stability conditions to be undertaken. Our results show that disordered proteins have lower transition temperatures (Fig. 2) and faster kinetic

rates (Fig. 6). Alsallaq and Zhou have suggested that the association constants of unstructured proteins will be substantially lower than those of folded proteins by extending their transition-state theory of rigid-body protein–protein associations to unstructured proteins.⁵⁶ All-atom binding simulations of the wide-type p53–MDM2 complex and various mutants have revealed that increasing the helicity of p53 increases binding affinity by about 4 kcal/mol.⁵⁷ Although details describing how disorder affects binding affinity are not clear in our current study, the kinetic advantages (partially) account for why IDPs have rapid turnover rates and are extensively enrolled in transcription and translation regulation and cellular signal transduction events.

IDPs were found in this study to be less stable while possessing greater binding/unbinding rates. The observations are consistent with a recent study by Vamvaca *et al.*, where the kinetics and thermodynamics of a ligand binding to a native enzyme and an engineered molten globular enzyme have been detected.²⁵ Estimated from k_{obs} , the disordered molten globular enzyme was found to have a ligand binding rate threefold greater than that of the native counterpart. The stabilization of the α -helix in free p27 with alanine substitutions has been found to slow the rate of the formation of the complex with cyclin A–Cdk2 by threefold.⁵⁸ This result indicates that the absence of a preformed helix contributes beneficially to p27-inhibitory activity. Although not included in our simulations, electrostatic interactions are important for ultrasensitive binding of IDPs⁵⁹ and have been shown to promote binding speed significantly by sharply decreasing binding free-energy barriers.³⁶

For protein folding, folding and unfolding rates can be estimated from the height of free-energy barrier by transition-state theory when the fraction of native contacts (Q) is used as reaction coordinate. Such an estimate of folding/unfolding rates is usually consistent with those obtained from direct kinetic simulations.^{60–63} However, our results indicate this may not always be the case in the protein binding problem. In our simulations, the binding free-energy barrier for the most ordered system ($\alpha=8.0$) is $2.4k_B T$ higher than that for the most disordered system ($\alpha=0.1$) (Fig. 4). Using the same method as that used in the protein folding problem to estimate the binding kinetics, we expected disordered proteins to have a binding rate 11 times as fast as that of the ordered proteins. This value is almost fourfold the result obtained by our direct kinetic simulations. Taking into account translational diffusion does not remove the apparent discrepancy. The ratio of the binding rate of the disordered proteins ($\alpha=0.1$) to the binding rate of the ordered proteins ($\alpha=8.0$) is 2.5 when using the mass–center distance (ΔR) as reaction coordinate. This is consistent with the results obtained from direct binding simulations. However, the inclusion of diffusion will remove this consistency. Although Q_b is widely used in protein binding problems,^{35–37,64} our results

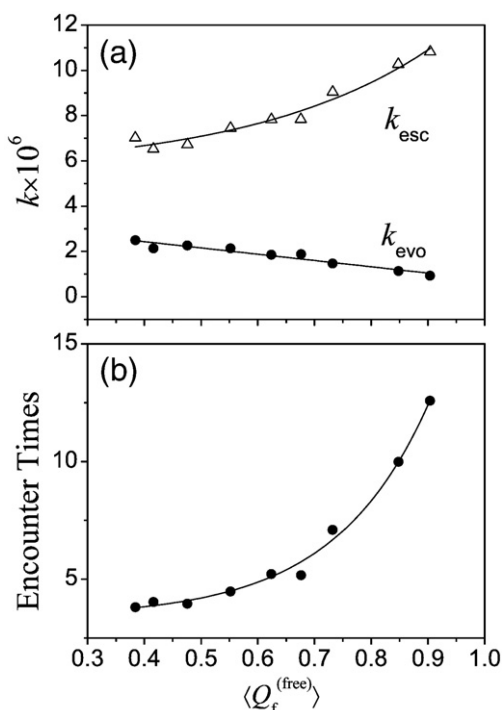


Fig. 7. Decomposition of the binding kinetics for the pKID–KIX complex with various chain flexibilities at T_m . (a) Transition rates of the encounter intermediate (pKID–KIX) either escape to the unbound state (k_{esc} ; open triangles) or evolve to the native bound state (k_{evo} ; filled circles). (b) Average encounter times in successful binding as a function of chain flexibility. Four hundred binding trajectories are averaged for each data point.

indicate that this parameter is not a good reaction coordinate for describing the binding process. Q_b cannot discriminate different states within the unbound states and the nonnative encounter complex, whereas it can monitor the evolution process from the encounter state to the bound state. In contrast, although the ΔR value can provide the relative distance between the two free proteins, it provides little information about the coupled folding–binding process. Hence, Q_b and ΔR do not fully describe the binding process alone; however, the two parameters complement each other to provide a better description of the binding process. Clearly, reaction coordinates that describe the binding process more accurately are required.

In a binding process where a ligand is captured to form a loosely bound complex (encounter complex) and subsequently always evolves to the final complex, the binding rate would be approximately equal to the capture rate. This assumption has been widely adopted to interpret the kinetic advantages of IDPs in terms of their greater capture radii. However, our simulations reveal that multiple capture events usually exist in one binding trajectory, and the kinetic advantage of IDPs most likely arises from the fewer encounter times to reach the final bound complex. Further experiments are needed to clarify the microscopic picture of the

coupled folding–binding of IDPs. Single-molecule spectroscopy⁶⁵ and NMR techniques²¹ may provide valuable information at this level.

In our simulations, we have studied the coupled folding–binding process of IDPs. However, not all IDPs become fully ordered upon binding.⁴⁸ Limited by our current model, we did not obtain information on these cases directly. The main features of binding revealed from our simulations (i.e., IDPs have a slower diffusion rate, fewer encounter times, and a lower thermodynamic stability) are related to chain disorder rather than folding upon binding, so we speculate that these features are general and will be shared by all IDPs. Further work is needed to test it.

Conclusion

The collection of experimental data on protein binding showed that IDPs bind to their targets with greater rates than ordered proteins. To explore the possible origins of the kinetic advantages of IDPs, we modified a continuum explicit-chain model by introducing a parameter α to scale the intrachain interaction strength. Using this modified model, we continuously tuned the pKID domain from the disordered state to the ordered state. The thermodynamics and kinetics of the pKID–KIX binding/unbinding process were demonstrated to be critically different between disordered and ordered systems. IDPs bind to targets coupled with folding through the “fly-casting” mechanism, whereas ordered proteins dock to their targets. IDPs have greater effective capture radius and can weakly bind to targets from a larger distance. However, IDPs also show greater hydrodynamic radii and, therefore, slower diffusion rates. The kinetic advantage of greater capture radii is negated by a decrease in diffusion rate, which results in slower encounter rates of IDPs. Nonetheless, the simulations indicate that IDPs show kinetic advantages over ordered proteins due to fewer encounter times required to produce the bound complex from the unbound state. Although widely used in protein binding problems, our results indicate that both fractions of the native interchain contacts Q_b and the distance between the mass centers of the two chains ΔR can only partially describe the features of the binding process, and better reaction coordinates are required to accurately describe the binding process.

Models and Method

Native-centric Gō-like model

In our simulations, native-centric Gō-like potentials^{66,67} were used. Despite simplifications and limitations,⁶⁸ Gō-like potentials have been widely used in protein folding simulations^{55,69–73} and recently have been applied to protein binding,^{35,36,64,74} and they have provided valuable insights into the thermodynamics and kinetics of protein

folding and binding problems. In the model system we considered (the pKID–KIX complex), two protein chains were included. For simplicity, the ordered target protein (the KIX domain) was kept frozen during simulations, while the disordered part (the pKID domain) was free to move. Thus, the Gō-like potential energy for the pKID–KIX complex with a continuum C^α chain representation is proposed as:

$$\begin{aligned}
 V_{\text{total}} &= V_{\text{stretching}}^{\text{pKID}} + V_{\text{bending}}^{\text{pKID}} + V_{\text{torsion}}^{\text{pKID}} + V_{\text{non-bonded}}^{\text{pKID}} + V_{\text{non-bonded}}^{\text{pKID-KIX}} \\
 &= \sum_{\text{bonds}} K_r (r - r_0)^2 + \sum_{\text{angles}} K_\theta (\theta - \theta_0)^2 \\
 &\quad + \sum_{\text{dihedrals}} \left\{ K_\phi^{(1)} [1 - \cos(\phi - \phi_0)] \right. \\
 &\quad \left. + K_\phi^{(3)} [1 - \cos 3(\phi - \phi_0)] \right\} \\
 &\quad + \alpha \left\{ \sum_{i < j - 3, \text{native}}^{\text{pKID}} \varepsilon \left[5 \left(\frac{r'_{ij}}{r_{ij}} \right)^{12} - 6 \left(\frac{r'_{ij}}{r_{ij}} \right)^{10} \right] \right. \\
 &\quad \left. + \sum_{i < j - 3, \text{non-native}}^{\text{pKID}} \varepsilon \left(\frac{r_{\text{rep}}}{r_{ij}} \right)^{12} \right\} \\
 &\quad + \sum_{i, j, \text{native}}^{\text{pKID-KIX}} \varepsilon \left[5 \left(\frac{r'_{ij}}{r_{ij}} \right)^{12} - 6 \left(\frac{r'_{ij}}{r_{ij}} \right)^{10} \right] \\
 &\quad + \sum_{i, j, \text{non-native}}^{\text{pKID-KIX}} \varepsilon \left(\frac{r_{\text{rep}}}{r_{ij}} \right)^{12}
 \end{aligned} \tag{3}$$

where the total energy is divided into bond stretching, angle bending, torsion, and nonbonded interactions. r , θ , and ϕ are, respectively, the virtual bond length, bond angle, and torsion angles defined by C^α atom positions. Nonbonded interactions were only considered when two C^α atoms i and j are separated sequentially by at least three residues within one chain or when they come from, and were subdivided into native and nonnative parts. For native interactions, a 12–10 Lennard–Jones form potential was used, where r_{ij} is the virtual nonbonded spatial distance between C^α atoms i and j . For nonnative interactions, r_{rep} parameterizes the excluded volume repulsion between residue pairs that do not belong to the given native contact set. r_0 , θ_0 , ϕ_0 , and r'_{ij} are the corresponding native values available from the Protein Data Bank structure. Parameter settings in Kaya and Chan⁵⁵ and Liu and Chan⁷⁵ were used in this work, namely, $r_{\text{rep}} = 4.0$ Å, $K_r = 100\varepsilon$, $K_\theta = 20\varepsilon$, $K_\phi^{(1)} = \varepsilon$, and $K_\phi^{(3)} = 0.5\varepsilon$. Interaction strength is controlled by the parameter ε . In order to continuously tune the degree of disorder of pKID domain, we introduced the parameter α into the potential function to scale the intrachain interaction strength.

To build our model system, we used the NMR structure of the pKID–KIX complex (Protein Data Bank code 1KDX).²⁰ A native contact set was built based on the CSU software.⁷⁶ Since the KIX domain was kept frozen in the simulations, only the intrachain native contacts within the pKID domain were counted. The native contact set based on the CSU software gives 25 intrachain native contacts within the pKID domain and 50 interchain native contacts between pKID and KIX. The fraction of native intrachain (folding) contacts Q_f was used to monitor the folding process, and the fraction of native interchain (binding) contacts Q_b was used to monitor the binding process.

Thermodynamics and kinetic simulations

The coupled folding–binding process was simulated by Langevin dynamics.⁷⁷ The equation of motion is:

$$m \ddot{v}(t) = F_{\text{conf}}(t) - m\gamma v(t) + \eta(t) \tag{4}$$

where m , \ddot{v} , F_{conf} , γ , v , η , and t are the mass, acceleration, conformational force, friction constant, velocity, random force, and time, respectively. As in Kaya and Chan, units were chosen such that $m = 1$ and timescale was controlled by the quantity $\tau = \sqrt{ma^2/\varepsilon_0}$, where the length scale a was set to 4 Å and the reference energy scale ε_0 was set 1.⁵⁵ Friction constant γ was set $1.00\tau^{-1}$, which lies in the overdamped region. The molecular dynamics time step $\delta t = 0.005\tau$ was used in numerical integration. Simulation times were reported in units of δt .

Simulations on the coupled folding–binding process were conducted by placing a pKID chain and a KIX chain in cubic boxes with different sizes (ranging from 150 to 250 Å, according to a solution concentration of ~500–100 μM). Periodic boundary conditions were applied on all three directions. The KIX domain was kept frozen at the box center, while the pKID domain was free to move. For thermodynamic conformational sampling, standard histogram techniques, with appropriate bias potentials, were adopted. For unbinding simulations, 400 trajectories, which started from the native bound structure with different initial velocities, were collected. Binding simulations were carried out using 400 randomly chosen unbound structures from the unbinding simulation at a higher temperature.

To evaluate the diffusion process of free pKID, a pKID molecule was placed in an infinitely large box without periodic boundary conditions and was free to diffuse. Long timescale diffusions (5,000,000 steps) were carried out with the same settings used in the coupled folding–binding simulations. The average fraction of native intrachain contacts of pKID in the free form (Q_f^{free}) was used to measure the degree of disorder.

Experimental kinetic data for IDPs and ordered proteins

Nonexhaustive kinetic data for IDPs and ordered proteins were collected from the literature. Data are summarized in Tables 1 and 2. These data have been detected under various solution and technical conditions, namely, fluorescence correlation spectroscopy, spectrophotometric assay (SA), surface plasmon resonance (SPR), stopped flow (SF), resonant mirror biosensor (RMB), scintillation proximity-based assay, quartz crystal microbalance (QCM), NMR ¹⁵N R_2 dispersions, and radioligand binding assay (RBA). Detection methods that were not clearly stated in the original article are marked “not clear.” Data were divided into the disordered group and the ordered group. As long as one of the binding partners was disordered or partially disordered, the complex was grouped into the disordered class.

Acknowledgements

This work was supported by the Ministry of Science and Technology of China (grant 2009CB918500) and the National Natural Science Foundation of

China (grant 10721403). The authors thank Huan-Xiang Zhou, Daqi Yu, and Meng Gao for helpful discussions.

References

1. Wright, P. E. & Dyson, H. J. (1999). Intrinsically unstructured proteins: re-assessing the protein structure–function paradigm. *J. Mol. Biol.* **293**, 321–331.
2. Oldfield, C. J., Cheng, Y., Cortese, M. S., Brown, C. J., Uversky, V. N. & Dunker, A. K. (2005). Comparing and combining predictors of mostly disordered proteins. *Biochemistry*, **44**, 1989–2000.
3. Ward, J. J., Sodhi, J. S., McGuffin, L. J., Buxton, B. F. & Jones, D. T. (2004). Prediction and functional analysis of native disorder in proteins from the three kingdoms of life. *J. Mol. Biol.* **337**, 635–645.
4. Cheng, Y., LeGall, T., Oldfield, C. J., Dunker, A. K. & Uversky, V. N. (2006). Abundance of intrinsic disorder in protein associated with cardiovascular disease. *Biochemistry*, **45**, 10448–10460.
5. Haynes, C., Oldfield, C. J., Ji, F., Klitgord, N., Cusick, M. E., Radivojac, P. *et al.* (2006). Intrinsic disorder is a common feature of hub proteins from four eukaryotic interactomes. *PLoS Comput. Biol.* **2**, e100.
6. Liu, J., Perumal, N. B., Oldfield, C. J., Su, E. W., Uversky, V. N. & Dunker, A. K. (2006). Intrinsic disorder in transcription factors. *Biochemistry*, **45**, 6873–6888.
7. Dunker, A. K., Brown, C. J., Lawson, J. D., Iakoucheva, L. M. & Obradović, Z. (2002). Intrinsic disorder and protein function. *Biochemistry*, **41**, 6573–6582.
8. Fuxreiter, M., Tompa, P., Simon, I., Uversky, V. N., Hansen, J. C. & Asturias, F. J. (2008). Malleable machines take shape in eukaryotic transcriptional regulation. *Nat. Chem. Biol.* **4**, 728–737.
9. Dyson, H. J. & Wright, P. E. (2005). Intrinsically unstructured proteins and their functions. *Nat. Rev. Mol. Cell Biol.* **6**, 197–208.
10. Dyson, H. J. & Wright, P. E. (2002). Coupling of folding and binding for unstructured proteins. *Curr. Opin. Struct. Biol.* **12**, 54–60.
11. Kriwacki, R. W., Hengst, L., Tennant, L., Reed, S. I. & Wright, P. E. (1996). Structural studies of p21Waf1/Cip1/Sdi1 in the free and Cdk2-bound state: conformational disorder mediates binding diversity. *Proc. Natl Acad. Sci. USA*, **93**, 11504–11509.
12. Goldberg, J. M. & Baldwin, R. L. (1998). Kinetic mechanism of a partial folding reaction: 1. Properties of the reaction and effects of denaturants. *Biochemistry*, **37**, 2546–2555.
13. Narayanan, R., Ganesh, O. K., Edison, A. S. & Hagen, S. J. (2008). Kinetics of folding and binding of an intrinsically disordered protein: the inhibitor of yeast aspartic proteinase YPrA. *J. Am. Chem. Soc.* **130**, 11477–11485.
14. Anderluh, G., Gökce, I. & Lakey, J. H. (2004). A natively unfolded toxin domain uses its receptor as a folding template. *J. Biol. Chem.* **279**, 22002–22009.
15. Vise, P. D., Baral, B., Latos, A. J. & Daughdrill, G. W. (2005). NMR chemical shift and relaxation measurements provide evidence for the coupled folding and binding of the p53 transactivation domain. *Nucleic Acids Res.* **33**, 2061–2077.
16. Klages, J., Kotsch, A., Coles, M., Sebald, W., Nickel, J., Müller, T. & Kessler, H. (2008). The solution structure of BMPR-1A reveals a local disorder-to-order transition upon BMP-2 binding. *Biochemistry*, **47**, 11930–11939.
17. Sugase, K., Lansing, J. C., Dyson, H. J. & Wright, P. E. (2007). Tailoring relaxation dispersion experiments for fast-associating protein complexes. *J. Am. Chem. Soc.* **129**, 13406–13407.
18. Chrivia, J. C., Kwok, R. P. S., Lamb, N., Hagiwara, M., Montminy, M. R. & Goodman, R. H. (1993). Phosphorylated CREB binds specifically to the nuclear protein CBP. *Nature*, **365**, 855–859.
19. Mestas, S. P. & Lumb, K. J. (1999). Electrostatic contribution of phosphorylation to the stability of the CREB–CBP activator–coactivator complex. *Nat. Struct. Mol. Biol.* **6**, 613–614.
20. Radhakrishnan, I., Pérez-Alvarado, G. C., Parker, D., Dyson, H. J., Montminy, M. R. & Wright, P. E. (1997). Solution structure of the KIX domain of CBP bound to the transactivation domain of CREB: a model for activator:coactivator interactions. *Cell*, **91**, 741–752.
21. Sugase, K., Dyson, H. J. & Wright, P. E. (2007). Mechanism of coupled folding and binding of an intrinsically disordered protein. *Nature*, **447**, 1021–1025.
22. Gunasekaran, K., Tsai, C. -J., Kumar, S., Zanuy, D. & Nussinov, R. (2003). Extended disordered proteins: targeting function with less scaffold. *Trends Biochem. Sci.* **28**, 81–85.
23. Uversky, V. N., Oldfield, C. J. & Dunker, A. K. (2005). Showing your ID: intrinsic disorder as an ID for recognition, regulation and cell signaling. *J. Mol. Recognit.* **18**, 343–384.
24. Shoemaker, B. A., Portman, J. J. & Wolynes, P. G. (2000). Speeding molecular recognition by using the folding funnel: the fly-casting mechanism. *Proc. Natl Acad. Sci. USA*, **97**, 8868–8873.
25. Vamvaca, K., Jelesarov, I. & Hilvert, D. (2008). Kinetics and thermodynamics of ligand binding to a molten globular enzyme and its native counterpart. *J. Mol. Biol.* **382**, 971–977.
26. Muralidhara, B. K., Rathinakumar, R. & Wittung-Stafshede, P. (2006). Folding of *Desulfovibrio desulfuricans* flavodoxin is accelerated by cofactor fly-casting. *Arch. Biochem. Biophys.* **451**, 51–58.
27. Lengyel, C. S. E., Willis, L. J., Mann, P., Baker, D., Kortemme, T., Strong, R. K. & McFarland, B. J. (2007). Mutations designed to destabilize the receptor-bound conformation increase MICA–NKG2D association rate and affinity. *J. Biol. Chem.* **282**, 30658–30666.
28. Crespin, M. O., Boys, B. L. & Konermann, L. (2005). The reconstitution of unfolded myoglobin with hemin dicyanide is not accelerated by fly-casting. *FEBS Lett.* **579**, 271–274.
29. Hoffman, R. M. B., Blumenschein, T. M. A. & Sykes, B. D. (2006). An interplay between protein disorder and structure confers the Ca²⁺ regulation of striated muscle. *J. Mol. Biol.* **361**, 625–633.
30. Perham, M., Chen, M., Ma, J. & Wittung-Stafshede, P. (2005). Unfolding of heptameric co-chaperonin protein follows “fly casting” mechanism: observation of transient nonnative heptamer. *J. Am. Chem. Soc.* **127**, 16402–16403.
31. Jemth, P. & Gianni, S. (2007). PDZ domains: folding and binding. *Biochemistry*, **46**, 8701–8708.
32. Landfried, D. A., Vuletich, D. A., Pond, M. P. & Lecomte, J. T. J. (2007). Structural and thermodynamic consequences of *b* heme binding for monomeric apoglobins and other apoproteins. *Gene*, **398**, 12–28.

33. Onitsuka, M., Kamikubo, H., Yamazaki, Y. & Kataoka, M. (2008). Mechanism of induced folding: both folding before binding and binding before folding can be realized in staphylococcal nuclease mutants. *Proteins Struct. Funct. Bioinf.* **72**, 837–847.
34. Wang, J., Zhang, K., Lu, H. & Wang, E. (2006). Dominant kinetic paths on biomolecular binding–folding energy landscape. *Phys. Rev. Lett.* **96**, 168101.
35. Turjanski, A. G., Gutkind, J. S., Best, R. B. & Hummer, G. (2008). Binding-induced folding of a natively unstructured transcription factor. *PLoS Comput. Biol.* **4**, e1000060.
36. Levy, Y., Onuchic, J. N. & Wolynes, P. G. (2007). Fly-casting in protein–DNA binding: frustration between protein folding and electrostatics facilitates target recognition. *J. Am. Chem. Soc.* **129**, 738–739.
37. Gupta, N. & Irbäck, A. (2004). Coupled folding–binding versus docking: a lattice model study. *J. Chem. Phys.* **120**, 3983–3989.
38. Papoian, G. A. & Wolynes, P. G. (2003). The physics and bioinformatics of binding and folding—an energy landscape perspective. *Biopolymers*, **68**, 333–349.
39. Levy, Y., Cho, S. S., Onuchic, J. N. & Wolynes, P. G. (2005). A survey of flexible protein binding mechanisms and their transition states using native topology based energy landscapes. *J. Mol. Biol.* **346**, 1121–1145.
40. Coluzza, I. & Frenkel, D. (2007). Monte Carlo study of substrate-induced folding and refolding of lattice proteins. *Biophys. J.* **92**, 1150–1156.
41. Verkhivker, G. M., Bouzida, D., Gehlhaar, D. K., Rejto, P. A., Freer, S. T. & Rose, P. W. (2003). Simulating disorder–order transitions in molecular recognition of unstructured proteins: where folding meets binding. *Proc. Natl Acad. Sci. USA*, **100**, 5148–5153.
42. Tsai, C. -J., Kumar, S., Ma, B. & Nussinov, R. (1999). Folding funnels, binding funnels, and protein function. *Protein Sci.* **8**, 1181–1190.
43. Hilser, V. J. & Thompson, E. B. (2007). Intrinsic disorder as a mechanism to optimize allosteric coupling in proteins. *Proc. Natl Acad. Sci. USA*, **104**, 8311–8315.
44. Zhou, H. -X. (2005). How do biomolecular systems speed up and regulate rates? *Phys. Biol.* **2**, R1–R25.
45. Karplus, M. & McCammon, J. A. (2002). Molecular dynamics simulations of biomolecules. *Nat. Struct. Mol. Biol.* **9**, 646–652.
46. Abeln, S. & Frenkel, D. (2008). Disordered flanks prevent peptide aggregation. *PLoS Comput. Biol.* **4**, e1000241.
47. Radhakrishnan, I., Pérez-Alvarado, G. C., Dyson, H. J. & Wright, P. E. (1998). Conformational preferences in the Ser133-phosphorylated and non-phosphorylated forms of the kinase inducible transactivation domain of CREB. *FEBS Lett.* **430**, 317–322.
48. Okazaki, K. -I. & Takada, S. (2008). Dynamic energy landscape view of coupled binding and protein conformational change: induced-fit versus population-shift mechanisms. *Proc. Natl Acad. Sci. USA*, **105**, 11182–11187.
49. Fuxreiter, M., Simon, I., Friedrich, P. & Tompa, P. (2004). Preformed structural elements feature in partner recognition by intrinsically unstructured proteins. *J. Mol. Biol.* **338**, 1015–1026.
50. Mohan, A., Oldfield, C. J., Radivojac, P., Vacic, V., Cortese, M. S., Dunker, A. K. & Uversky, V. N. (2006). Analysis of molecular recognition features (MoRFs). *J. Mol. Biol.* **362**, 1043–1059.
51. Yoon, M. -K., Venkatachalam, V., Huang, A., Choi, B. -S., Stultz, C. M. & Chou, J. J. (2009). Residual structure within the disordered C-terminal segment of p21Waf1/Cip1/Sdi1 and its implications for molecular recognition. *Protein Sci.* **18**, 337–347.
52. Wang, J., Zhang, K., Lu, H. & Wang, E. (2006). Quantifying the kinetic paths of flexible biomolecular recognition. *Biophys. J.* **91**, 866–872.
53. Schreiber, G., Haran, G. & Zhou, H. -X. (2009). Fundamental aspects of protein–protein association kinetics. *Chem. Rev.* **109**, 839–860.
54. Uversky, V. N. (2002). Natively unfolded proteins: a point where biology waits for physics. *Protein Sci.* **11**, 739–756.
55. Kaya, H. & Chan, H. S. (2003). Solvation effects and driving forces for protein thermodynamic and kinetic cooperativity: how adequate is native-centric topological modeling? *J. Mol. Biol.* **326**, 911–931.
56. Alsallaq, R. & Zhou, H. -X. (2007). Energy landscape and transition state of protein–protein association. *Biophys. J.* **92**, 1486–1502.
57. Dastidar, S. G., Lane, D. P. & Verma, C. S. (2008). Multiple peptide conformations give rise to similar binding affinities: molecular simulations of p53-MDM2. *J. Am. Chem. Soc.* **130**, 13514–13515.
58. Bienkiewicz, E. A., Adkins, J. N. & Lumb, K. J. (2002). Functional consequences of preorganized helical structure in the intrinsically disordered cell-cycle inhibitor p27(Kip1). *Biochemistry*, **41**, 752–759.
59. Borg, M., Mittag, T., Pawson, T., Tyers, M., Forman-Kay, J. D. & Chan, H. S. (2007). Polyelectrostatic interactions of disordered ligands suggest a physical basis for ultrasensitivity. *Proc. Natl Acad. Sci. USA*, **104**, 9650–9655.
60. Du, R., Pande, V. S., Grosberg, A. Y., Tanaka, T. & Shakhnovich, E. S. (1998). On the transition coordinate for protein folding. *J. Chem. Phys.* **108**, 334–350.
61. Cho, S. S., Levy, Y. & Wolynes, P. G. (2006). P versus Q: structural reaction coordinates capture protein folding on smooth landscapes. *Proc. Natl Acad. Sci. USA*, **103**, 586–591.
62. Chavez, L. L., Onuchic, J. N. & Clementi, C. (2004). Quantifying the roughness on the free energy landscape: entropic bottlenecks and protein folding rates. *J. Am. Chem. Soc.* **126**, 8426–8432.
63. Wallin, S. & Chan, H. S. (2006). Conformational entropic barriers in topology-dependent protein folding: perspectives from a simple native-centric polymer model. *J. Phys. Condens. Matter*, **18**, S307–S328.
64. Wang, J., Lu, Q. & Lu, H. P. (2006). Single-molecule dynamics reveals cooperative binding–folding in protein recognition. *PLoS Comput. Biol.* **2**, e78.
65. Lu, H. P. (2005). Probing single-molecule protein conformational dynamics. *Acc. Chem. Res.* **38**, 557–565.
66. Go, N. (1983). Theoretical studies of protein folding. *Annu. Rev. Biophys. Bioeng.* **12**, 183–210.
67. Ueda, Y., Taketomi, H. & Gö, N. (1978). Studies on protein folding, unfolding, and fluctuations by computer simulation: II. A three-dimensional lattice model of lysozyme. *Biopolymers*, **17**, 1531–1548.
68. Clementi, C. & Plotkin, S. S. (2004). The effects of nonnative interactions on protein folding rates: theory and simulation. *Protein Sci.* **13**, 1750–1766.
69. Liu, Z. & Chan, H. S. (2005). Desolvation is a likely origin of robust enthalpic barriers to protein folding. *J. Mol. Biol.* **349**, 872–889.

70. Micheletti, C., Banavar, J. R., Maritan, A. & Seno, F. (1999). Protein structures and optimal folding from a geometrical variational principle. *Phys. Rev. Lett.* **82**, 3372–3375.
71. Shea, J. -E., Onuchic, J. N. & Brooks, C. L. (1999). Exploring the origins of topological frustration: design of a minimally frustrated model of fragment B of protein A. *Proc. Natl Acad. Sci. USA*, **96**, 12512–12517.
72. Koga, N. & Takada, S. (2001). Roles of native topology and chain-length scaling in protein folding: a simulation study with a G α -like model. *J. Mol. Biol.* **313**, 171–180.
73. Badasyan, A., Liu, Z. & Chan, H. S. (2008). Probing possible downhill folding: native contact topology likely places a significant constraint on the folding cooperativity of proteins with ~40 residues. *J. Mol. Biol.* **384**, 512–530.
74. Levy, Y., Wolynes, P. G. & Onuchic, J. N. (2004). Protein topology determines binding mechanism. *Proc. Natl Acad. Sci. USA*, **101**, 511–516.
75. Liu, Z. & Chan, H. S. (2005). Solvation and desolvation effects in protein folding: native flexibility, kinetic cooperativity and enthalpic barriers under isostability conditions. *Phys. Biol.*, S75–S85.
76. Sobolev, V., Sorokine, A., Prilusky, J., Abola, E. & Edelman, M. (1999). Automated analysis of interatomic contacts in proteins. *Bioinformatics*, **15**, 327–332.
77. Veitshans, T., Klimov, D. & Thirumalai, D. (1997). Protein folding kinetics: timescales, pathways and energy landscapes in terms of sequence-dependent properties. *Fold. Des.* **2**, 1–22.
78. Varghese, L. T., Sinha, R. K. & Irudayaraj, J. (2008). Study of binding and denaturation dynamics of IgG and anti-IgG using dual color fluorescence correlation spectroscopy. *Anal. Chim. Acta*, **625**, 103–109.
79. Castro, M. J. M. & Anderson, S. (1996). Alanine point-mutations in the reactive region of bovine pancreatic trypsin inhibitor: effects on the kinetics and thermodynamics of binding to β -trypsin and α -chymotrypsin. *Biochemistry*, **35**, 11435–11446.
80. Tello, D., Eisenstein, E., Schwarz, F. P., Goldbaum, F. A., Fields, B. A., Mariuzza, R. A. & Poljak, R. J. (1994). Structural and physicochemical analysis of the reaction between the anti-lysozyme antibody D1.3 and the anti-idiotopic antibodies E225 and E5.2. *J. Mol. Recognit.* **7**, 57–62.
81. Kelley, R. F., Costas, K. E., O'Connell, M. P. & Lazarus, R. A. (1995). Analysis of the factor VIIa binding site on human tissue factor: effects of tissue factor mutations on the kinetics and thermodynamics of binding. *Biochemistry*, **34**, 10383–10392.
82. Johanson, K., Appelbaum, E., Doyle, M., Hensley, P., Zhao, B., Abdel-Meguid, S. S. *et al.* (1995). Binding interactions of human interleukin 5 with its receptor α subunit. *J. Biol. Chem.* **270**, 9459–9471.
83. Cunningham, B. C. & Wells, J. A. (1993). Comparison of a structural and a functional epitope. *J. Mol. Biol.* **234**, 554–563.
84. Wu, H., Myszka, D. G., Tendian, S. W., Brouillette, C. G., Sweet, R. W., Chaiken, I. M. & Hendrickson, W. A. (1996). Kinetic and structural analysis of mutant CD4 receptors that are defective in HIV gp120 binding. *Proc. Natl Acad. Sci. USA*, **93**, 15030–15035.
85. Myszka, D. G., Sweet, R. W., Hensley, P., Brigham-Burke, M., Kwong, P. D., Hendrickson, W. A. *et al.* (2000). Energetics of the HIV gp120–CD4 binding reaction. *Proc. Natl Acad. Sci. USA*, **97**, 9026–9031.
86. Singha, N. C., Vlamis-Gardikas, A. & Holmgren, A. (2003). Real-time kinetics of the interaction between the two subunits, *Escherichia coli* thioredoxin and gene 5 protein of phage T7 DNA polymerase. *J. Biol. Chem.* **278**, 21421–21428.
87. Raman, C. S., Jemmerson, R., Nall, B. T. & Allen, M. J. (1992). Diffusion-limited rates for monoclonal antibody binding to cytochrome *c*. *Biochemistry*, **31**, 10370–10379.
88. Yu, X., Wang, Q. -Y., Guo, Y., Dolmer, K., Young, J. A. T., Gettins, P. G. W. & Rong, L. (2003). Kinetic analysis of binding interaction between the subgroup A Rous sarcoma virus glycoprotein SU and its cognate receptor Tva: calcium is not required for ligand binding. *J. Virol.* **77**, 7517–7526.
89. Potempa, J., Kwon, K., Chawla, R. & Travis, J. (1989). Inter- α -trypsin inhibitor. inhibition spectrum of native and derived forms. *J. Biol. Chem.* **264**, 15109–15114.
90. Nielsen, P. K., Bønsager, B. C., Berland, C. R., Sigurskjold, B. W. & Svensson, B. (2003). Kinetics and energetics of the binding between barley α -amylase/subtilisin inhibitor and barley α -amylase 2 analyzed by surface plasmon resonance and isothermal titration calorimetry. *Biochemistry*, **42**, 1478–1487.
91. Bowman, B. F., Peterson, J. A. & Stull, J. T. (1992). Pre-steady-state kinetics of the activation of rabbit skeletal muscle myosin light chain kinase by Ca²⁺/calmodulin. *J. Biol. Chem.* **267**, 5346–5354.
92. England, P., Brégégère, F. & Bedouelle, H. (1997). Energetic and kinetic contributions of contact residues of antibody D1.3 in the interaction with lysozyme. *Biochemistry*, **36**, 164–172.
93. Schreiber, G. & Fersht, A. R. (1993). Interaction of barnase with its polypeptide inhibitor barstar studied by protein engineering. *Biochemistry*, **32**, 5145–5150.
94. Silversmith, R. E., Levin, M. D., Schilling, E. & Bourret, R. B. (2008). Kinetic characterization of catalysis by the chemotaxis phosphatase CheZ: modulation of activity by the CheYp substrate. *J. Biol. Chem.* **283**, 756–765.
95. Xavier, K. A., McDonald, S. M., McCammon, J. A. & Willson, R. C. (1999). Association and dissociation kinetics of bobwhite quail lysozyme with monoclonal antibody HyHEL-5. *Protein Eng.* **12**, 79–83.
96. Li, X., Fong, C. -C., Huang, M., Cao, H., Zhao, J. & Yang, M. (2008). Measurement of binding kinetics between PI3-K and phosphorylated IGF-1R using a surface plasmon resonance biosensor. *Microchim. Acta*, **162**, 253–260.
97. Fridmann, Y., Kafri, G., Danziger, O. & Horovitz, A. (2002). Dissociation of the GroEL–GroES asymmetric complex is accelerated by increased cooperativity in ATP binding to the GroEL ring distal to GroES. *Biochemistry*, **41**, 5938–5944.
98. Murphy, A. J., Kemp, F. & Love, J. (2008). Surface plasmon resonance characterization of caldesmon–calmodulin binding kinetics. *Anal. Biochem.* **376**, 61–72.
99. Razai, A., Garcia-Rodriguez, C., Lou, J., Geren, I. N., Forsyth, C. M., Robles, Y. *et al.* (2005). Molecular evolution of antibody affinity for sensitive detection of botulinum neurotoxin type A. *J. Mol. Biol.* **351**, 158–169.
100. Wu, H., Pfarr, D. S., Tang, Y., An, L. -L., Patel, N. K., Watkins, J. D. *et al.* (2005). Ultra-potent antibodies against respiratory syncytial virus: effects of binding

- kinetics and binding valence on viral neutralization. *J. Mol. Biol.* **350**, 126–144.
101. Solheim, S. A., Petsalaki, E., Stokka, A. J., Russell, R. B., Taskén, K. & Berge, T. (2008). Interactions between the Fyn SH3-domain and adaptor protein CBP/PAG derived ligands, effects on kinase activity and affinity. *FEBS J.* **275**, 4863–4874.
 102. Swope, S. L. & Haganir, R. L. (1994). Binding of the nicotinic acetylcholine receptor to SH2 domains of Fyn and Fyk protein tyrosine kinases. *J. Biol. Chem.* **269**, 29817–29824.
 103. Rich, R. L., Cannon, M. J., Jenkins, J., Pandian, P., Sundaram, S., Magyar, R. *et al.* (2008). Extracting kinetic rate constants from surface plasmon resonance array systems. *Anal. Biochem.* **373**, 112–120.
 104. Lavery, D. N. & McEwan, I. J. (2008). Functional characterization of the native NH₂-terminal transactivation domain of the human androgen receptor: binding kinetics for interactions with TFIIF and SRC-1a. *Biochemistry*, **47**, 3352–3359.
 105. Lambert, B. & Buckle, M. (2006). Characterisation of the interface between nucleophosmin (NPM) and p53: potential role in p53 stabilisation. *FEBS Lett.* **580**, 345–350.
 106. Spoerner, M., Herrmann, C., Vetter, I. R., Kalbitzer, H. R. & Wittinghofer, A. (2001). Dynamic properties of the Ras switch I region and its importance for binding to effectors. *Proc. Natl Acad. Sci. USA*, **98**, 4944–4949.
 107. Curmi, P. A., Andersen, S. S. L., Lachkar, S., Gavet, O., Karsenti, E., Knossow, M. & Sobel, A. (1997). The stathmin/tubulin interaction *in vitro*. *J. Biol. Chem.* **272**, 25029–25036.
 108. Ishino, T., Pasut, G., Scibek, J. & Chaiken, I. (2004). Kinetic interaction analysis of human interleukin 5 receptor α mutants reveals a unique binding topology and charge distribution for cytokine recognition. *J. Biol. Chem.* **279**, 9547–9556.
 109. Abdiche, Y., Malashock, D., Pinkerton, A. & Pons, J. (2008). Determining kinetics and affinities of protein interactions using a parallel real-time label-free biosensor, the Octet. *Anal. Biochem.* **377**, 209–217.
 110. Keeler, C., Jablonski, E. M., Albert, Y. B., Taylor, B. D., Myszk, D. G., Clevenger, C. V. & Hodsdon, M. E. (2007). The kinetics of binding human prolactin, but not growth hormone, to the prolactin receptor vary over a physiologic pH range. *Biochemistry*, **46**, 2398–2410.
 111. Zaccheo, O. J., Prince, S. N., Miller, D. M., Williams, C., Kemp, C. F., Brown, J. *et al.* (2006). Kinetics of insulin-like growth factor II (IGF-II) interaction with domain 11 of the human IGF-II/mannose 6-phosphate receptor: function of CD and AB loop solvent-exposed residues. *J. Mol. Biol.* **359**, 403–421.
 112. Albeck, S. & Schreiber, G. (1999). Biophysical characterization of the interaction of the β -lactamase TEM-1 with its protein inhibitor BLIP. *Biochemistry*, **38**, 11–21.
 113. Wohlgemuth, S., Kiel, C., Krämer, A., Serrano, L., Wittinghofer, F. & Herrmann, C. (2005). Recognizing and defining true Ras binding domains: I. Biochemical analysis. *J. Mol. Biol.* **348**, 741–758.
 114. Nakajima, H., Cocquerel, L., Kiyokawa, N., Fujimoto, J. & Levy, S. (2005). Kinetics of HCV envelope proteins' interaction with CD81 large extracellular loop. *Biochem. Biophys. Res. Commun.* **328**, 1091–1100.
 115. Portmann, R., Magnani, D., Stoyanov, J. V., Schmelch, A., Multhaup, G. & Solioz, M. (2004). Interaction kinetics of the copper-responsive CopY repressor with the *cop* promoter of *Enterococcus hirae*. *J. Biol. Inorg. Chem.* **9**, 396–402.
 116. Panayotou, G., Gish, G., End, P., Truong, O., Gout, I., Dhand, R. *et al.* (1993). Interactions between SH2 domains and tyrosine-phosphorylated platelet-derived growth factor, β -receptor sequences: analysis of kinetic parameters by a novel biosensor-based approach. *Mol. Cell. Biol.* **13**, 3567–3576.
 117. Ladbury, J. E., Hensmann, M., Panayotou, G. & Campbell, I. D. (1996). Alternative modes of tyrosyl phosphopeptide binding to a Src family SH2 domain: implications for regulation of tyrosine kinase activity. *Biochemistry*, **35**, 11062–11069.
 118. Chen, T., Repetto, B., Chizzonite, R., Pullar, C., Burghardt, C., Dharm, E. *et al.* (1996). Interaction of phosphorylated Fc ϵ RI γ immunoglobulin receptor tyrosine activation motif-based peptides with dual and single SH2 domains of p72syk. assessment of binding parameters and real time binding kinetics. *J. Biol. Chem.* **271**, 25308–25315.
 119. Chook, Y. M., Gish, G. D., Kay, C. M., Pai, E. F. & Pawson, T. (1996). The Grb2–mSos1 complex binds phosphopeptides with higher affinity than Grb2. *J. Biol. Chem.* **271**, 30472–30478.
 120. Nominé, Y., Botuyan, M. V., Bajzer, Z., Owen, W. G., Caride, A. J., Wasielewski, E. & Mer, G. (2008). Kinetic analysis of interaction of BRCA1 tandem breast cancer C-terminal domains with phosphorylated peptides reveals two binding conformations. *Biochemistry*, **47**, 9866–9879.
 121. Rudolph, M. G., Bayer, P., Abo, A., Kuhlmann, J., Vetter, I. R. & Wittinghofer, A. (1998). The Cdc42/Rac interactive binding region motif of the Wiskott Aldrich syndrome protein (WASP) is necessary but not sufficient for tight binding to Cdc42 and structure formation. *J. Biol. Chem.* **273**, 18067–18076.
 122. Waxham, M. N., Tsai, A.-L. & Putkey, J. A. (1998). A mechanism for calmodulin (CaM) trapping by CaM-kinase II defined by a family of CaM-binding peptides. *J. Biol. Chem.* **273**, 17579–17584.
 123. Anderlüh, G., Hong, Q., Boetzel, R., MacDonald, C., Moore, G. R., Virden, R. & Lakey, J. H. (2003). Concerted folding and binding of a flexible colicin domain to its periplasmic receptor TolA. *J. Biol. Chem.* **278**, 21860–21868.
 124. Garcia, K. C., Radu, C. G., Ho, J., Ober, R. J. & Ward, E. S. (2001). Kinetics and thermodynamics of T cell receptor–autoantigen interactions in murine experimental autoimmune encephalomyelitis. *Proc. Natl Acad. Sci. USA*, **98**, 6818–6823.
 125. Woodside, D. G., Obergfell, A., Talapatra, A., Calderwood, D. A., Shattil, S. J. & Ginsberg, M. H. (2002). The N-terminal SH2 domains of Syk and ZAP-70 mediate phosphotyrosine-independent binding to integrin β cytoplasmic domains. *J. Biol. Chem.* **277**, 39401–39408.
 126. Krantz, B. A., Moran, L. B., Kentsis, A. & Sosnick, T. R. (2000). D/H amide kinetic isotope effects reveal when hydrogen bonds form during protein folding. *Nat. Struct. Mol. Biol.* **7**, 62–71.
 127. Dürr, E., Jelesarov, I. & Bosshard, H. R. (1999). Extremely fast folding of a very stable leucine zipper with a strengthened hydrophobic core and lacking electrostatic interactions between helices. *Biochemistry*, **38**, 870–880.
 128. Ibarra-Molero, B., Makhatadze, G. I. & Matthews, C. R. (2001). Mapping the energy surface for the folding reaction of the coiled-coil peptide GCN4-p1. *Biochemistry*, **40**, 719–731.

129. Steinmetz, M. O., Jelesarov, I., Matousek, W. M., Honnappa, S., Jahnke, W., Missimer, J. H. *et al.* (2007). Molecular basis of coiled-coil formation. *Proc. Natl Acad. Sci. USA*, **104**, 7062–7067.
130. Wendt, H., Berger, C., Baici, A., Thomas, R. M. & Bosshard, H. R. (1995). Kinetics of folding of leucine zipper domains. *Biochemistry*, **34**, 4097–4107.
131. Matsuno, H., Furusawa, H. & Okahata, Y. (2004). Kinetic study of phosphorylation-dependent complex formation between the kinase-inducible domain (KID) of CREB and the KIX domain of CBP on a quartz crystal microbalance. *Chem. Eur. J.* **10**, 6172–6178.
132. Zanier, K., Charbonnier, S., Baltzinger, M., Nominé, Y., Altschuh, D. & Travé, G. (2005). Kinetic analysis of the interactions of human papillomavirus E6 oncoproteins with the ubiquitin ligase E6AP using surface plasmon resonance. *J. Mol. Biol.* **349**, 401–412.
133. Baggio, R., Carven, G. J., Chiulli, A., Palmer, M., Stern, L. J. & Arenas, J. E. (2005). Induced fit of an epitope peptide to a monoclonal antibody probed with a novel parallel surface plasmon resonance assay. *J. Biol. Chem.* **280**, 4188–4194.
134. Schon, O., Friedler, A., Bycroft, M., Freund, S. M. V. & Fersht, A. R. (2002). Molecular mechanism of the interaction between MDM2 and p53. *J. Mol. Biol.* **323**, 491–501.
135. Catimel, B., Teh, T., Fontes, M. R. M., Jennings, I. G., Jans, D. A., Howlett, G. J. *et al.* (2001). Biophysical characterization of interactions involving importin- α during nuclear import. *J. Biol. Chem.* **276**, 34189–34198.
136. Gianni, S., Engström, Å., Larsson, M., Calosci, N., Malatesta, F., Eklund, L. *et al.* (2005). The kinetics of PDZ domain–ligand interactions and implications for the binding mechanism. *J. Biol. Chem.* **280**, 34805–34812.